This is a repository copy of *Interfacial Particle Dynamics: One and Two Step Yielding in Colloidal Glass.*.

White Rose Research Online URL for this paper:
http://eprints.whiterose.ac.uk/109961/

Version: Accepted Version

Interfacial particle dynamics: One and two step yielding in colloidal glass

Huagui Zhang*, Kai Yu, Olivier J. Cayre and David Harbottle*

School of Chemical and Process Engineering, University of Leeds, LS2 9JT, UK

Corresponding authors:

D. Harbottle: Email: d.harbottle@leeds.ac.uk, Phone: +44 (0) 113 343 4154;

H. Zhang: Email: prehz@leeds.ac.uk

ABSTRACT

The yielding behaviour of silica nanoparticles partitioned at an air-aqueous interface is reported. Linear viscoelasticity of the particle-laden interface can be retrieved via a time-dependent and electrolyte-dependent superposition, and the applicability of the 'soft glassy rheology' (SGR) model is confirmed. With increasing electrolyte concentration (φ^{elect}) a non-ergodic state is achieved with particle dynamics arrested firstly from attraction induced bonding bridges and then from the cage effect of particle jamming, manifesting in a two-step yielding process under large amplitude oscillation strain (LAOS). The Lissajous curves disclose a shear-induced in-cage particle re-displacement within oscillation cycles between the two yielding steps, exhibiting a 'strain softening' transitioning to 'strain stiffening' as the interparticle attraction increases. By varying φ^{elect} and the particle spreading concentration, φ^{SiO_2}, a variety of phase transitions from fluid- to gel- and glass-like can be unified to construct a state diagram mapping the yielding behaviors from one-step to two-step before finally exhibiting one-step yielding at high φ^{elect} and φ^{SiO_2}.

1. INTRODUCTION

Colloidal particles partitioned at the gas/liquid or liquid/liquid interface, known as two-dimensional (2D) colloids, are of great interest particularly due to their crucial role in stabilizing foams and emulsions which find broad application in fields such as cosmetics,

pharmaceuticals and oil recovery, to name just a few[1, 2]. These particle networks also provide the foundation for novel materials synthesis in 2D geometry such as porous textures[3], 2D arrays of nanocrystals[4], microcapsules[5], bijels[6], catalyst supports and filters[7, 8]. In most applications the shear rheology of the particle-laden interface greatly influences the macroscopic performance of multiphase systems, especially the stability of emulsions and foams in dynamic environments[9, 10]. The shear-induced deformation of emulsion droplets and foam bubbles, as well as the liquid drainage in the plateau-borders, can be strongly influenced by the degree of particle mobility and reorganization at the interface[11-13]. It has also been reported that the arrested coalescence of bubbles/droplets is related to the shear yield strength of the interfacial layer, as the deformation and breakup of the bubble/droplet is limited by the rigidity of the interface[14]. Nevertheless, fundamental understanding of the particles' interfacial dynamics remains largely unexplored and knowledge is often extrapolated from three-dimensional (3D) particle dispersions. For instance, yielding, a ubiquitous property in material science and engineering that is often considered as a feature of phase transition[15], is generally studied in bulk, particularly for colloidal gels or concentrated suspensions, but receives much less attention with regard to the shear induced flow transitions of adsorbed or spread interfacial layers[16]. The advancement of interfacial science and the development of novel materials highlight the need to explore further the yielding phenomenon and the yielding state diagram of particle-laden interfaces.

It is well-known that state transitions in 3D soft solids are related to the number of particle-particle contacts (i.e. particle concentration), and the strength of interaction between neighboring particles (often described by the classical DLVO theory[17, 18]). For example, increasing the particle volume fraction (ϕ) leads to a transition from the equilibrium state of a liquid to a non-ergodic glassy state as ϕ exceeds ~ 0.59. In the glassy state the particles are 'caged' by their neighbours with their long-range diffusion restricted by the overcrowded volume[19]. This restriction effect of particle diffusion can also be observed at low ϕ when the short-range attraction between particles is strong, for example depletion attraction induced by non-adsorbing polymers[20], and van der Waals attraction induced by weakening electrical double layer repulsion forces[20, 21]. Particularly in dispersions of high ϕ and strong particle attraction, the so-called attractive driven glass (ADG), both caged and bonding effects exist which manifest in a two-step yielding process[20]. Two-step yielding often occurs in systems with two competing length-scales and/or time-scales of interaction[16]. Experimentally it can be challenging to explore this two-step yielding due to the possible crystallization and sample

preparation difficulties at high ϕ for hard sphere systems[22, 23]. The phenomena of two-step yielding has also been observed in colloidal suspensions of deformable microgels where the yielding is dependent on the particle softness[16].

With the introduction of interfacial shear geometries, several pioneering studies have considered the shear and yielding dynamics of different surface active species including globular proteins[24], silica nanoparticles[25], ultrathin nano-crystalline films[26] and asphaltenes[27, 28] at the air/water or oil/water interface. For 2D particle-laden interfaces the shear viscoelasticity is greatly dependent on the ability for particles to remain attached at the gas/liquid or liquid/liquid interface. Both the particle size and wettability have been shown to adjust the particle detachment energy, with strong particle attachment observed when the particle contact angle approaches 90° and the particle size is maximized (although the gravitational force contribution should be negligible). Particle aggregation enhanced by the addition of electrolyte not only modifies the apparent particle size but also increases slightly the wettability of the particle[29]. Both effects contribute to the increased retention of particles at the gas/liquid or liquid/liquid interface, and hence modify the interfacial rheology[30]. From the viewpoint of interparticle forces, the dielectric difference between the two liquid phases produce a counter-ion distribution asymmetry around the particle, and a dipolar repulsion can emerge to alter the nature of the particle interaction at the interface[31]. This contribution, weakly controllable by the electrolyte concentration, further affects the particle aggregation at the interface and hence the surface rheology.

Moreover, in practice, particle-laden interfaces of emulsions and foams encounter large shear flows which promote significant interfacial deformation, so the non-linear viscoelasticity of the particle-laden interface better represents the response of an interface in dynamic environments. Large-amplitude oscillatory shear (LAOS) enables the measurement of shear-induced melting (yielding) of soft matter materials under large strain. The complexity of the microscopic mechanics in the non-linear flow regime and especially the correlation to the shear-induced structure remains poorly understood. For instance, the microscopic origin of non-linearity associated with yielding in particulate systems, which reflects cage deformation, breaking and particle displacement is largely unexplored. Some insights into the mechanics of non-linear rheology have been highlighted through studying polymer and particle dispersions[32, 33]. Even for model hard-sphere (HS) colloids, the relationship between structure and particle dynamics beyond the linear viscoelastic response has not been revealed until recent work by Koumakis et al.,[34] using a combination of oscillatory shear rheometry and

Brownian dynamics (BD) simulation. The authors reported a complex yielding phenomenon for the HS glasses, which was attributed to cage escape dominated by the particles' Brownian motion, and/or cage breaking dominated by shear-assisted particle collisions, dependent on the flow regime (i.e. Peclet numbers). Complete understanding of the structural relaxation mechanism of out-of-cage motion induced by large flows is often challenged by interference between the complex kinematic history and the non-linear response of the system[35]. For systems which include short-range attraction, as in the current study, the non-linear response becomes more complex due to contributions from both cage and bond breaking. While it is complex to visualize the microscopic yielding mechanics, structural rearrangements can be inferred from the stress and dissipative energy responses of the system. For particle-laden interfaces, research considering the yielding mechanics remain few and far between[9], although some understanding of particle rearrangement in the plastic regime of 2D jammed colloids has recently been described[36].

In the current study we investigate the interfacial dynamics of deposited sub-50 nm silica nanoparticles at the air-water interface. The interparticle interaction potential was tuned by simply adjusting the electrolyte concentration in the aqueous subphase, and the number of particle-particle contacts altered by varying the deposited particle concentration. Interfacial shear rheology in small- and large-amplitude oscillations has been performed to demonstrate the effects of both the electrolyte and particle concentration on the surface viscoelasticity and the shear yielding of the particle-laden interface. The 'soft glassy rheology' (SGR) model is used to rationalize the linear viscoelasticity of the particle-laden interface, and information drawn from Lissajous plots is used to describe the particle reconfiguration during the yielding processes. Moreover, a state diagram has been constructed to map the yielding behaviour (one- or two-step) of the particle-laden interface as a function of the network phase, i.e. fluid-like through solid-gel to jamming glass.

2. EXPERIMENTAL METHODS

2.1 Materials: Ludox AS40 silica nanoparticles (NPs) were obtained from Sigma-Aldrich (UK) as a 40 wt% particle dispersion in water. Before use the dispersion was ion exchanged using Amberlite IRN 50 resin to remove counter-ions NH_4^+ and diluted to 10 wt% using Milli-Q water. The extraction of counter-ions was verified by conductivity measurements. Ultrapure Milli-Q water was used in all experiments with a resistivity of 18.2 MΩ·cm.

Isopropyl alcohol (IPA) and sodium sulphate (99%+ A.C.S. grade, Sigma Aldrich, UK) were used as received without further purification.

2.2 Particle-air-water three phase contact angle: To approximate the effect of electrolyte concentration on the particle contact angle, sessile drop measurements were conducted by placing a ~10 µL droplet of the brine solution on a glass substrate. The silica glass was cleaned by sonication in 2 wt% Decon solution (anionic surfactant) for 10 min and then rinsed with Milli-Q water and acetone before drying using nitrogen. The droplet contact angle was measured using the supplier software of the Attension Theta tensiometer, KSV. As the wettability measurements are known to be sensitive to the substrate chemical composition and roughness[37], statistical confidence in the observed trend was improved by conducting a minimum of 10 sessile drop experiments at different locations on the glass substrate.

2.3 Particle size and zeta potential: The hydrodynamic diameter and zeta potential of the silica particles in the presence of electrolyte were measured using the Zeta NanoSizer (Malvern Instruments, UK). Three repeat measurements were completed and the error bars shown in Figure 1b confirm the maximum and minimum variability associated with the three samples. In the absence of any electrolyte the Ludox silica particle diameter was 34 nm with a PDI of 0.14.

2.4 Interfacial shear rheology: The shear rheology of the air-aqueous interface laden with particles was measured using a stress-controlled Discovery Hybrid Rheometer (DHR-2) (TA Instruments, UK) equipped with a Double Wall Ring (DWR) geometry[38]. To achieve maximum measurement sensitivity the instrument was calibrated using precision mapping with the transducer bearing mode set to soft. 19.2 mL aqueous subphase (φ^{elect} varied between 5 mM and 2 M) was gently pipetted in the circular Delrin trough to a level that the interface was pinned at the inner edge of the trough, minimizing any effect of the liquid meniscus. All interfacial rheology measurements were conducted without pH adjustment. Over the electrolyte concentrations studied, the aqueous pH remained in the range pH 5.5 to 5.7.

Prior to depositing particles at the air-aqueous interface, the ion-exchanged 10 wt% Ludox silica dispersion was diluted in the spreading solvent (isopropyl alcohol (IPA) + Milli-Q water (42/58 w/w)) to varying particle concentrations: 5.7 wt%, 1 wt%, 0.5 wt% and 0.1 wt% (based on the suspension mass). 100 µL of the desired particle dispersion was carefully spread at the air-aqueous interface to form a particle-laden interface. The DWR geometry was

flame cleaned and gently positioned to pin the air-aqueous interface. Prior to each measurement the spreading solvent was allowed to evaporate for 25 min. Strain amplitude sweep experiments were conducted in oscillation mode at an angular frequency of 0.5 rad/s. Dynamic frequency sweep tests were completed with the strain amplitude (γ_0) set to 0.03%, a value within the linear viscoelastic regime. All measurements were conducted at ambient conditions, T = 20.5 ^{o}C. More details on the rheological technique and experimental procedures can be found elsewhere[27].

To decouple the surface stress from the subphase bulk contribution the dimensionless Boussinesq number (Bo) is defined as the ratio of interfacial stress to bulk stress, and is given by:

$$B_o = \frac{\eta_s}{\eta L} \tag{1}$$

where η_s is the interfacial shear viscosity, η is the shear viscosity of subphase liquid, and L is a characteristic length scale determined by the probe geometry, defined as the ratio of the geometrical area to the perimeter on which stress is applied. For the DWR geometry L is 0.7 mm. At low Bo numbers (Bo << 1) the rheological response is dominated by the subphase contribution, only when Bo is high enough (Bo >> 1) the measured response represents the surface rheology. As demonstrated, correction of velocity profiles is necessary to decouple the subphase drag contribution for surface viscosities below 10^{-5} Pa·s·m (Bo ~ 14.3)[38]. In the present study, even in the most unfavorable case with the lowest measurable viscoelasticity (i.e. spreading φ^{SiO_2} = 5.7 wt% and φ^{elect} = 7 mM), the surface viscosity is greater than 10^{-5} Pa·s·m. Indeed, we have examined the contribution of subphase drag effect using the Matlab code kindly provided by Prof. Jan Vermant's group[38], and we find that the subphase contribution is negligible for all systems studied. Therefore, the raw experimental data is presented without further processing.

2.5 Imaging particle-laden interfacial layers

Particle-laden interfacial layers were deposited onto freshly cleaved mica (Electron Microscopy Sciences, Fisher Scientific, UK) using the Langmuir-Blodgett technique. The mica substrate was first submerged below the air-aqueous interface prior to depositing the particles. The system was equilibrated for 25 min to allow evaporation of the spreading solvent before the mica surface was gently withdrawn through the particle-laden interface at a rate of 90 mm/min. The deposited samples were dried in a desiccator before imaging using a

Field Emission Gun Scanning Electron Microscope (FEGSEMLEO1530 GEMINI, Carl Zeiss Inc).

3. RESULTS AND DISCUSSION

3.1 Particle-particle interactions at the air/aqueous interface

In bulk suspensions the colloidal structure is greatly related to the nature of interparticle forces, for example, crystalline order due to long-range repulsive forces, fractal-aggregates due to attractive forces, etc[23]. Hence, in light of the intimate structure-rheology relation, the interparticle interaction determines the flow behaviour of suspensions and acts as a key control parameter in phase transition. When colloidal particles, that intrinsically carry ionizable groups on their surface (like the silica nanoparticles used in the current study), are dispersed in water, the electrostatic repulsion arising from the surface charges and the van der Waals attraction between neighbouring particles dictate the stability and rheology of the suspension. However, for like-charged particles partitioned at an aqueous and low dielectric medium (e.g. air or oil) interface, the pairwise interaction energy $U(r)$ is modified from that typically described by the classical DLVO theory[17, 18]. Partial exposure of the particle in air enhances the van der Waals attraction potential which is given by:

$$U_{vdw}(r) = -AR/[12(r-2R)] \qquad (2)$$

with an effective Hamaker constant A. In this equation R is the particle radius and r is the particle center to center distance. The effective Hamaker constant as suggested by Williams and Berg[39] is considered in terms of $A = A_{pp} + f^2(3-2f)(A_{pwp} - A_{pp})$, where A_{pp} and A_{pwp} represent the particle Hamaker constants in air and water, respectively ($A_{pp} = 6.6 \times 10^{-20}$J[40], $A_{pwp} = 8.5 \times 10^{-21}$J for silica[23]), and f is the fractional immersion height as determined from the water contact angle θ (see Figure 1a). It is worth noting that the slight variability in measured contact angle for each electrolyte concentration may result from surface roughness effects[37]. In the current study, sessile droplet measurements were conducted on a glass slide which is known to be rougher than the more conventional silicon wafer. However, the overall trend of increasing contact angle with increasing electrolyte concentration is observed and supported by previously published data[29].
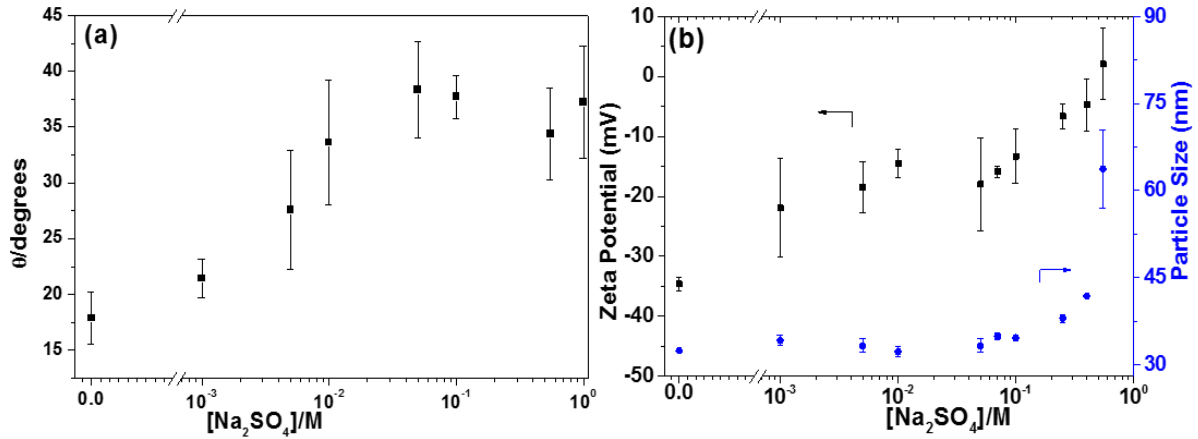
Figure 1. a) Contact angle of aqueous droplets at rest on a glass substrate as a function of the electrolyte concentration; **b)** Zeta potential and hydrodynamic diameter of silica particles dispersed in Na_2SO_4 solutions of varying concentration from 0 M to 0.55 M.

The interparticle electrostatic repulsion force at the air-water interface not only includes the short-range Coulomb contribution $U_{Co}(r)$, but also a long-range dipolar repulsion $U_{di}(r)$, which arises from the asymmetric counterion distribution due to the particle positioning in both phases[41, 42]. The Coulomb repulsive potential $U_{Co}(r)$ can be approximated by:

$$U_{Co}(r) = 2\pi\varepsilon_w R\psi_0^2 \exp[-\kappa(r - 2R)] \tag{3}$$

where ε_w is the dielectric constant of water, and ψ_0 is the particle surface potential, approximated by the zeta potential (see Figure 1b). κ^{-1} is the Debye length and is given by $\kappa^{-1} = (\varepsilon_w k_B T/1000 e^2 N_A 2I)^{1/2}$, where e is the elementary charge, N_A is Avogadro's number and I is the ionic strength. The dipolar repulsive potential $U_{di}(r)$ firstly derived by Hurd[43] using a linearization of the Poisson-Boltzmann equation, with $U_{di}(r) \propto \kappa^{-2}r^{-3}$, has been developed by Masschaele[41] replacing κ^{-1} with the finite size of the hydrated counterion a (the condensed Stern layer), and later revisited by Frydel et al.[44] considering the charge renormalization effect from polarization saturation of the neighboring fluid, giving the following equation[45]:

$$U_{di}(r) = \frac{(g_{wall} p_{point})^2}{8\pi\varepsilon_{air}} \left(\frac{1}{r}\right)^3 \tag{4}$$

with the renormalized dipole moment $p \approx g_{wall} p_{point}$ for small κ, where $p_{point} = 2q\kappa^{-1}\varepsilon_{air}/\varepsilon_w$, q is the total bound surface charge of the particle, and ε_{air} is the dielectric constant of air. The wall term of renormalization g_{wall} is expressed as:

$$g_{wall} = \left(\frac{e\sigma_c^2 a^3}{2\varepsilon_w k_B T} - \ln[a^3 c_s] \right) \Big/ \left(\frac{e\sigma_c}{\kappa\varepsilon_w k_B T} \right) \tag{5}$$

in which σ_c is the particle surface charge density, equal to 0.12 µC/cm^2 for silica[46], a value comparable to that determined on the basis of the experimentally measured zeta potential via $\sigma_c \approx \varepsilon_w \kappa \psi_0$; c_s is the number density of counterions in solution, and a is the ion's hydrated diameter, which is equal to 0.72 nm for sodium[45]. Note that the capillary force for nano-sized particles such as those used in the current study is negligible due to the uniform curvature and little restraint in the vertical direction[45]. The individual contributions from the attractive and repulsive forces (Eq. 2 to Eq. 4) are shown in Figure S1 (supporting information), and they are combined to calculate the overall interaction potential, $U_{Total}(r) = U_{vdw}(r) + U_{co}(r) + U_{di}(r)$, as shown in Figure 2a. The potentials are plotted in terms of U(h)/kT as a function of the particle separation distance (h = r − 2R), see inset of Figure 2a.
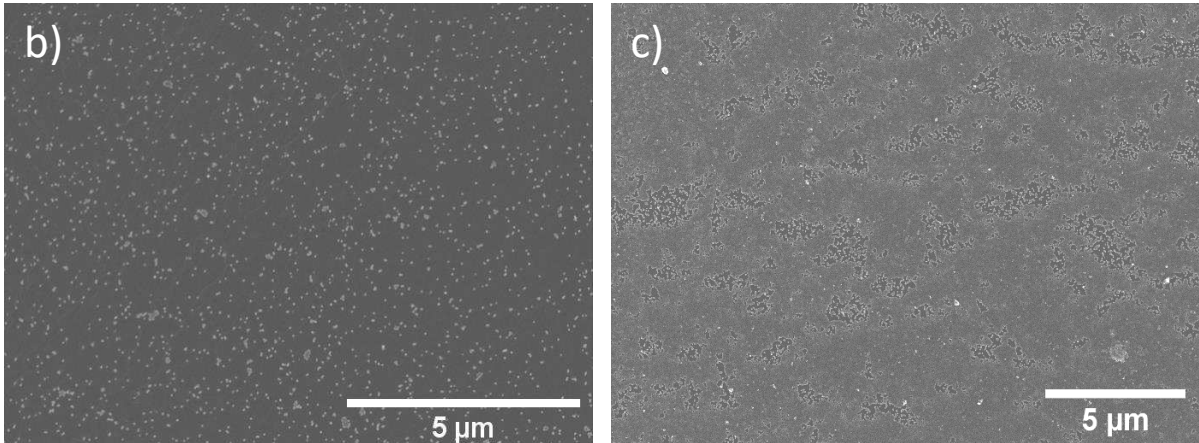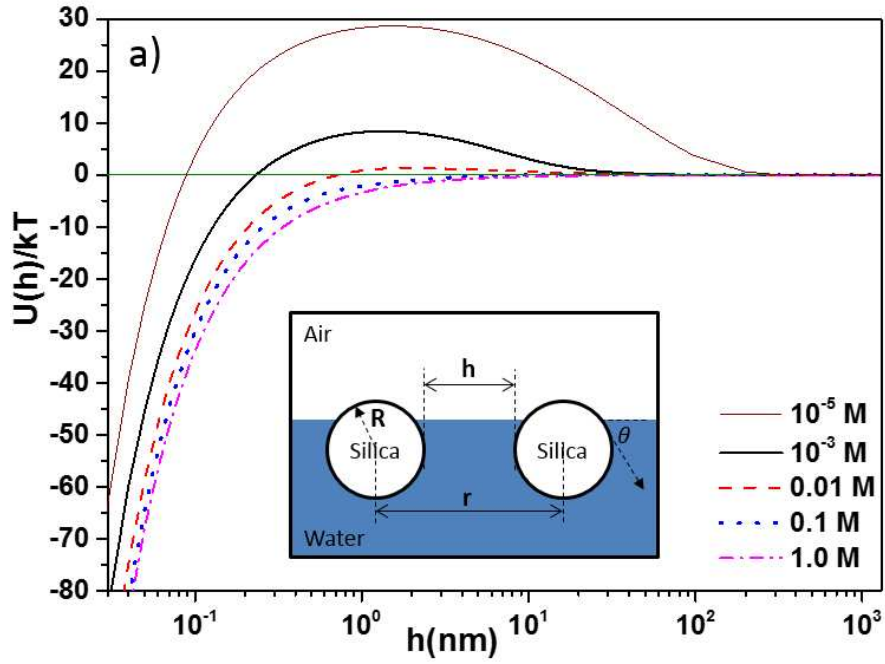
Figure 2. a) Silica particle-particle interaction potential (U(h)/kT) as a function of separation distance (h = r − 2R) and increasing φ^{elect} in the aqueous subphase; inset schematic of particles pinned at the air-aqueous interface. Scanning electron micrographs showing dispersive (subphase = 10^{-3} M Na_2SO_4, spreading φ^{SiO_2} = 5.7 wt%) **(b)**, and attractive (subphase = 0.01 M Na_2SO_4, spreading φ^{SiO_2} = 5.7 wt%) **(c)** particle network interactions.

As shown in Figure 2a, at low φ^{elect} the interparticle force is strongly repulsive exhibiting a high potential barrier against primary minimum aggregation. This is confirmed from the Scanning Electron Micrograph (SEM) of the deposited Langmuir-Blodgett (LB) layer (Figure 2b), where particle surface coverage remains low, Γ ~ 8% (determined using Image J software) for low φ^{elect} (e.g. 1 mM at φ^{SiO_2} = 5.7 wt%) or low φ^{SiO_2} (e.g. ⩽ 0.05 wt%).

With increasing φ^{elect} the repulsion potential is reduced to only a few k_BT when φ^{elect} = 0.01 M, enhancing the potential for particle-particle attraction and forming a near uniform particle monolayer when φ^{SiO_2} is high, e.g. 5.7 wt%, as shown in Figure 2c. Under this condition the particle surface coverage increases to $\sim 70\%$. High φ^{elect} not only increases the interparticle attraction strength but also the likelihood for particles to remain pinned at the air-aqueous interface due to the increase in interfacial adsorption energy, W_r [47]. Upon spreading, the potential for a particle to partition at the gas/liquid interface is dependent on W_r, which is a function of the surface tension γ, particle radius R, and three-phase contact angle θ via $\mathrm{W_r} = \gamma\mathrm{R}^2\pi(1\pm\cos\theta)^2$ [1]. A small increase in the particle size can significantly change $\mathrm{W_r}$ from only a few k_BT, where reversible interactions are influenced by thermal fluctuations, to several thousand k_BT where the particle adsorption is considered irreversible [1]. Hence, the ability for particles to remain at an interface can be enhanced through rapid surface aggregations, for instance cluster formation and growth via diffusion-limited cluster aggregation (DLCA)[23] resulting from an increase in φ^{elect}.
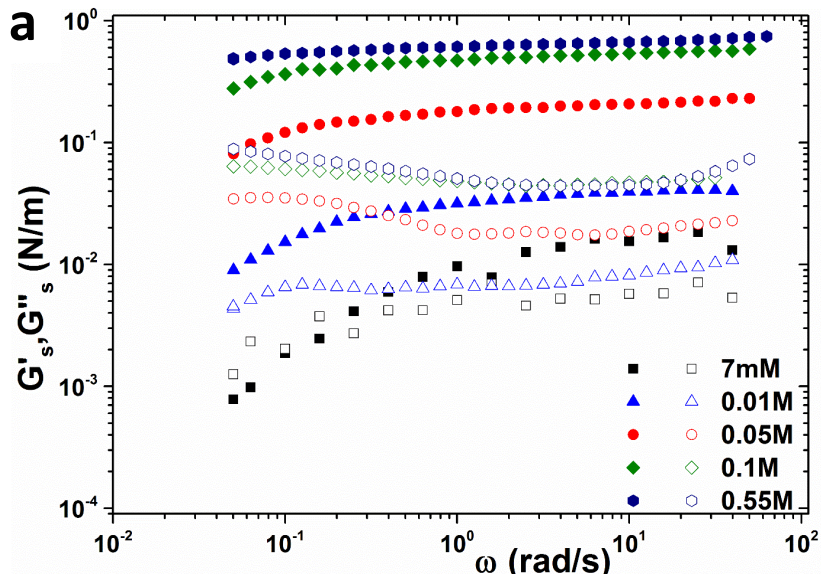
3.2 Linear viscoelasticity

To better understand the effect of the subphase electrolyte concentration (φ^{elect}) on the structural relaxation dynamics of the interfacial particle-laden layers, frequency-sweep tests were performed at a constant strain amplitude of 0.03%, within the linear viscoelastic regime, and the viscoelastic moduli G' and G" was measured as a function of the angular frequency, ω, varied between 0.05 and 50 rad/s. Depositing φ^{SiO_2} = 5.7 wt%, the interfacial viscoelasticity was unmeasurable until φ^{elect} equalled 7 mM. Below this critical condition, the particle surface coverage remains sufficiently low that the stress response of the system is below the sensitivity limit of the interfacial shear rheometer[23]. The viscoelastic responses of the particle-laden interfaces are shown in Figure 3a. It is evident that both G' and G" increase with increasing φ^{elect}, exhibiting an elastic dominance (i.e. G' > G") over the measured frequency range, except for 7 mM where a G'-G" crossover corresponding to a solid-like to liquid-like transition is measured as ω reduces. At 7 mM and 0.01 M, both G' and G" exhibit a power-law dependency in the low ω range equal to G'$\sim \omega^{0.7}$ and G"$\sim \omega^{0.6}$, and in the high ω range transition to a glassy state (G'$\sim \omega^0$). With increasing φ^{elect} the frequency dependence is weakened to a state where G' becomes almost independent of ω, and G" exhibits a more pronounced decrease with increasing ω.

The φ^{elect} influences the particle coverage at the air-aqueous interface and eventually a condition is satisfied when the particles 'jam' within a 'caged' state and their mobility is constrained by neighboring particles. The effect of φ^{elect} is somewhat equivalent to the frequency dependence on the viscoelastic moduli response of the interface. That is, in analogy to the well-known particle concentration-frequency superposition principle[24, 48], the frequency data can be scaled based on φ^{elect}, applying dependent horizontal (a_φ) and vertical (b_φ) shift factors to create a master curve according to the following equations:

$$b_\varphi G'(a_\varphi \omega) = G'_{ref}(\omega_{ref})$$

$$b_\varphi G''(a_\varphi \omega) = G''_{ref}(\omega_{ref}) \tag{6}$$

where subscript 'ref' is the reference φ^{elect}. As shown in Figure 3b the superposition is well achieved except for G" at high ω, which might be overestimated due to the hydrodynamic contribution from the subphase fluid, especially for low viscosity interfaces (i.e. at low φ^{elect}, thus G" at 7 mM is not considered for the superposition)[48]. The calculated shift factors a_φ and b_φ are displayed in the inset of Figure 3b. a_φ, which is proportional to the relaxation time of cage escape, experiences a transition when $\varphi^{elect} \sim 0.01$ M, signifying the approach to a glassy state where particles begin to undergo kinetic arrest. b_φ, which reflects the particle network strength, appears to transition towards a plateau as φ^{elect} approaches 0.55 M, and the glassy state is satisfied.
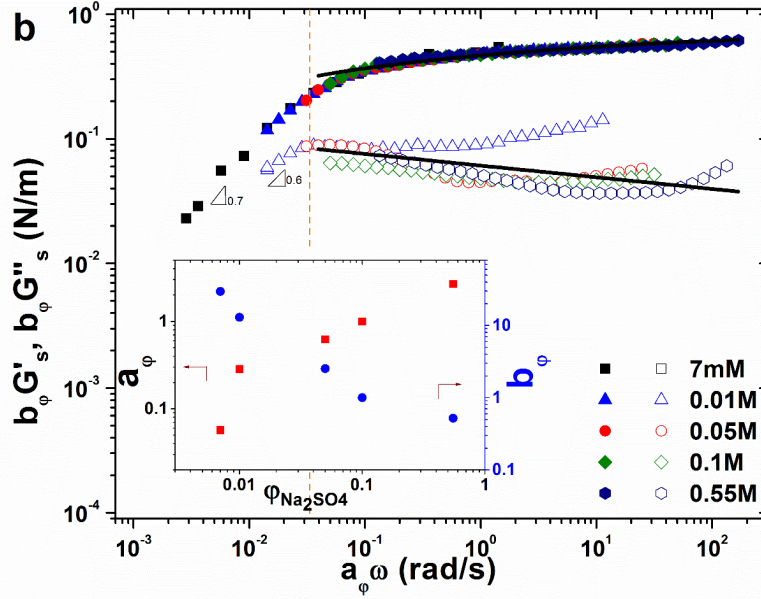
Figure 3. a) G' (closed symbols) and G'' (open symbols) frequency dependence for silica particles spread (φ^{SiO_2} = 5.7 wt%) at an air-aqueous interface (φ^{elect} varied between 7 mM and 0.55 M); **b)** G' (closed symbols) and G'' (open symbols) frequency dependence master curve created according to Eq. (6). Inset, horizontal and vertical shift factors versus φ^{elect}. Solid lines represent the best fit of the SGR model, and the dashed line differentiates between power-law dependency and glassy state.

The soft glassy rheology (SGR) model can be used to describe the linear viscoelastic dynamics of the interfacial particle layer, and the response is consistent with a range of other interfacially active species including polymers[49], carbon black particles[50] and asphaltenes[28], which are the polyaromatic heavy components of crude oil. The SGR model envisions a mesoscopic element scenario of 'particle trapping in a potential well', and the potential well depth represents the yielding energy barrier, which must be exceeded for particles to "hop" into a new configuration of lower overall energy[51, 52]. An effective noise temperature x, that is used to describe the interaction between different elements, controls the jamming extent and determines the rheological response of relaxation dynamics[30, 50, 53]. That is, for x > 3, the system exhibits Maxwell-like liquid behaviour, and for 1 < x < 3, the model predicts viscoelastic properties with $G' \sim \omega^{x-1}$ and $G'' \sim \omega^{x-1}$, as is the case for the low frequency dynamics (see Figure 3b). When x < 1, the system dynamics are frozen into a glassy state. To quantify the silica particle jamming at the air-aqueous interface we retrieve x by fitting the SGR model to the master curve in the high frequency region using equation:

$$\frac{G*(\omega, t)}{G_p} = 1 - \frac{1}{\Gamma(x)}(i\omega t)^{x-1} \qquad (7)$$

where G_p is the elasticity, t is the aging time (taken to be 1500 s), and $\Gamma(x)$ is the gamma function. The least square fitting lines shown in Figure 3b are equivalent to an interfacial modulus G_p of 0.88 N/m and a noise temperature x of 0.91, confirming the glassy state of the systems studied. Indeed, the glassy state is also verified by the power-law variation of $G(\omega)$, where G' exhibits a frequency independent plateau and G'' varies according to ω^{x-1}, thus satisfying the SGR model. Such an approach has recently been demonstrated by Masetro et al.[30] to test the glassy dynamics of colloidal particles.

3.3 Interfacial yielding behaviour

In general, the kinetic arrested structure can be broken by large amplitude oscillatory strain (LAOS) when a critical strain is imposed. This network yield can either be one-step or two-step depending on the two length scales of interparticle bonding and cage effect in the attractive colloidal network[15, 20, 34]. To reveal the yielding dynamics of the studied particle-laden interfaces, a sinusoidal shear deformation was imposed with its amplitude (γ_0) sweeping from 10^{-3} to 10^3 % at a constant angular frequency (0.5 rad/s). The measured interfacial shear stress (σ) and moduli (G' and G") versus strain amplitude (γ_0) are shown in Figure 4. For the systems considered, φ^{elect} and φ^{SiO_2} are the two variables governing the interparticle interaction strength and particle surface coverage, which dictates yielding behaviour. Figure 4b shows that for all electrolyte concentrations, 7 mM to 1 M Na_2SO_4, and $\varphi^{SiO_2} = 5.7$ wt%, the particle-laden interfaces are observed to be solid-like, elastically dominant (G' > G") at low strains (γ_0), followed by a solid-to-liquid transition (G' = G") at a critical γ_c, before both viscoelastic moduli decay at higher strain amplitudes. It is evident that for low φ^{elect} ($\leq$ 0.01 M) the yielding is featured as one-step considering the inflection-free power-law decay at higher strains beyond the G'-G" crossover. Such one-step yielding is also observed in Figure 4a, with a stress plateau above the critical strain γ_c, following an initial linear elastic solid response. This solid-to-liquid transition is also observed at higher φ^{elect} but the γ_c shifts from ~ 4% to ~ 0.3% with increasing φ^{elect}, a result of decreasing void domain size between particle clusters. For intermediate φ^{elect} (0.01 M ~ 0.55 M), where dense particle monolayers or even multilayers can be observed (see Figure S2), two-step yielding distinctly emerges, identified by two maxima or "shoulders" on the stress curve.

From Figure 4b, in proximity to the G'-G" crossover, a maximum peak of G" is observed and is associated to the energy dissipation during microstructural yielding. Moreover, unlike the inflection-free power-law decay for systems prepared at low φ^{elect}, an inflectional shoulder of G' and G" emerges, being identified as the second yielding point (the second yielding point is indicated by the arrows in Figure 4b). This response is very similar to the 3D attractive glass wherein a two-step yielding has also been reported[15, 16, 20, 54], although to the authors knowledge this is the first time two-step yielding has been reported for particle-laden interfacial layers.
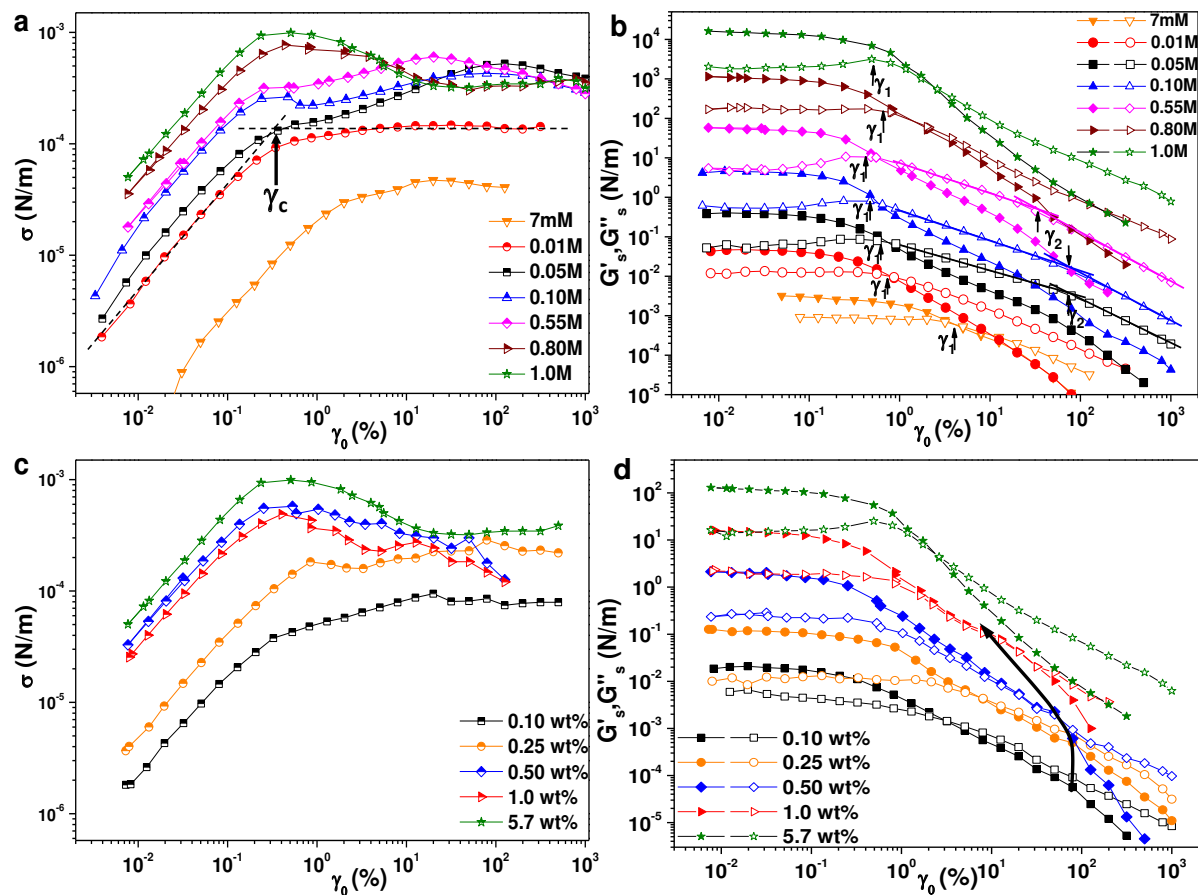

Figure 4. a) Stress (σ) versus strain amplitude (γ_0) response for silica particles partitioned at an air-aqueous interface as a function of the subphase electrolyte concentration φ^{elect}, varied between 7 mM and 1 M (particle spreading concentration φ^{SiO_2} fixed at 5.7 wt%); **b)** The corresponding viscoelastic (G" (open symbols) and G' (closed symbols)) responses versus γ_0. For clarity, the curves of 0.05 M, 0.1 M, 0.55 M, 0.8 M and 1 M have been vertically shifted using multiplication factors of 5, 25, 250, 2500 and 25000, respectively. Best fit lines have been included to easily identify the inflection points in the G" curves which correspond to the second yielding point. **c)** σ-γ_0 curves of the particle-laden interfaces with φ^{SiO_2} varying from

15

0.1 wt% to 5.7 wt% (φ^{elect} fixed at 1 M); **d)** The corresponding viscoelastic (G" (open symbols) and G' (closed symbols)) responses versus γ_0. For clarity, the curves of 0.25 wt% to 5.7 wt% have been vertically shifted using multiplication factors of 2.5, 5, 50 and 200, respectively. The arrow shows the shifting position of the second yielding (as featured by the second inflection point in G" curve).

The first yielding most likely relates to the disruption of the interparticle attractive bonds between clusters (a state that is also likely to be hypothesized as 'cages' for each test particle), and the second yielding relates to the breakage of the cluster as an instantaneous release of particles from the arrested state (cage breaking). While this is one possible explanation for the two-step yielding mechanism, further research to categorically elucidate the micro-structural changes under large strain is required. As φ^{elect} increases to 0.8 M, the second yielding broadens and is detected at a lower γ_0, while the first yielding remains almost independent of φ^{elect} (Figure 4a). In particular, the two yielding peaks are observed to merge into a single broader peak when $\varphi^{elect} \geq 0.8$ M, demonstrating reversibility to the one-step yielding process, similar to previously reported data when studying 3D systems of core-shell microgels[16]. Moreover, the inflection shoulders in both G' and G" curves are no longer identifiable, and one-step yielding is featured by a single peak in G". Transition back to one-step yielding results when the bonds between particles and clusters simultaneously break beyond the yielding stress or deformation, and this behaviour is observed when the particle-laden interface is densely packed with strong interaction forces acting between particles and clusters.

It might be suggested that the two-step yielding results from structural heterogeneity of the particle network at the air-aqueous interface. To eliminate any structural heterogeneity an amplitude sweep test was performed following a pre-shear protocol (2 s^{-1} × 3 min) to remove any influence resulting from the deposition method. The stress-strain responses shown in Figure S3 demonstrate good agreement between the particle-laden interfaces which have and have not undergone pre-shear prior to the amplitude sweep test. Hence, the deposition method does not measurably influence the yielding dynamics of the particle-laden interfaces. It is worth noting that pre-shear of the particle-laden interface may promote particle desorption into the aqueous sub-phase, as such the magnitude of the rheological response is slightly lowered.

Based on the φ^{elect} and φ^{SiO_2} dependent yielding behaviour (complementary data is shown in Figure S4), a state diagram can be constructed for the particle-laden interfaces, as depicted in Figure 5. When the φ^{elect} is below the critical electrolyte concentration, φ_c^{elect}, that confers detectable viscoelasticity by interfacial shear rheometry, the interfacial particle layer can be assumed to be in a liquid-like state. The φ_c^{elect} increases as φ^{SiO_2} decreases, defining the liquid-to-solid transition line. At conditions slightly above φ_c^{elect}, where the particle interface exhibits one-step yielding, the phase behavior of the particle-laden interface for low φ^{SiO_2} is identified as a gel before transitioning to the glassy state of particle jamming at higher φ^{SiO_2}. For high φ^{elect} and low φ^{SiO_2}, particle aggregation readily occurs via DLCA upon particle collisions[55], forming fractal clusters bridged via strong attractive bonds (schematically shown in Figure 7). This phase state can be considered to be an attractive gel which exhibits two-step yielding before transitioning to an attractive glass at high φ^{SiO_2} (see Figure 4c and 4d where one-step and two-step yielding can be identified either from the shoulder and/or peak in the σ curve, or from the features of G'' maximum peak and inflectional shoulders in the G' and G'' curves). For high concentrations (e.g. φ^{SiO_2} = 5.7 wt% and $\varphi^{elect} \geq 0.8$ M), the interparticle bond and cage break occur on a comparable time scale, thus exhibiting one-step yielding.
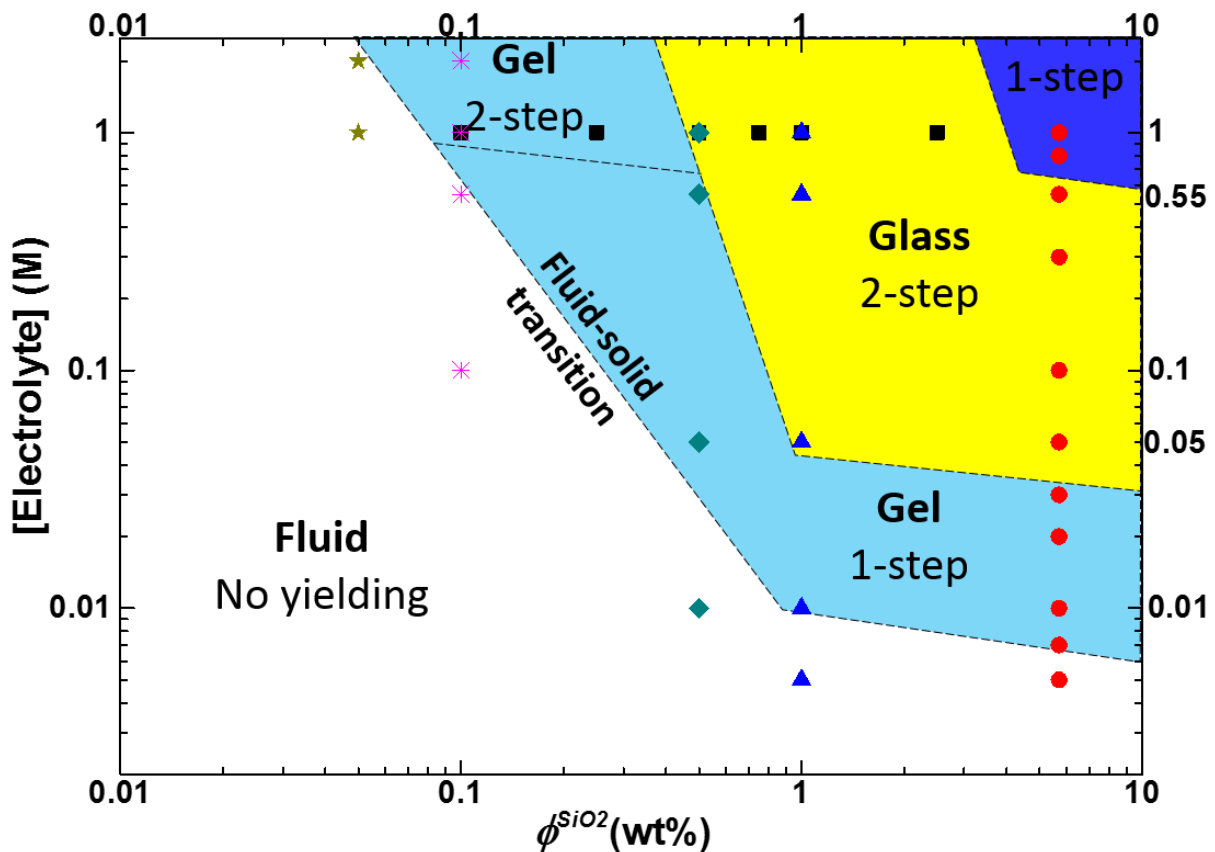
Figure 5. Yielding state diagram for silica nanoparticles partitioned at the air-aqueous interface with φ^{elect} and φ^{SiO_2} as varying parameters.

The intracycle stress response within a single oscillation provides useful information on the microstructural changes occurring when deformation exceeds the linear viscoelastic region, as encountered during large amplitude oscillatory strain (LAOS) [32]. For LAOS measurements, the intracycle interfacial stress waveforms and the imposed deformation function were recorded for each corresponding amplitude γ_0 studied in Figure 4. Figure 6 summarizes the non-linear response of the particle-laden interfaces in terms of Lissajous curves (intracycle stress versus strain), with closed stress-deformation loops. As is shown in Figure 6, transition from linear to non-linear viscoelastic response at the first yielding point (γ_1) is clearly manifested via distortion of the loop shape from an ellipse, indicative of the linear regime, to a progressive widening of the intracycle non-linearity as γ_0 increases beyond γ_1. Interestingly, for φ^{SiO_2} = 5.7 wt% and φ^{elect} = 0.05 M and 0.8 M, which show two-step and one-broad-step yielding respectively, the shape of the Lissajous loop in the non-linear regime is qualitatively different. The former exhibits classical transition from round shape indicative of a viscoelastic response, to a parallelogram intracycle pattern revealing plastic flow. For the latter, distortion from the elliptical shape in large γ_0 is featured with double symmetrical sharp upward corners at the end of the ellipse (in quadrants I and III), with the shape elongated along the y(stress)-axis before evolving into a final parallelogram shape reflecting plastic flow as γ_0 increases beyond the second yielding. The response equates to increased stress near the strain maximum, indicating a 'strain stiffening' of the sample within a period of oscillation.
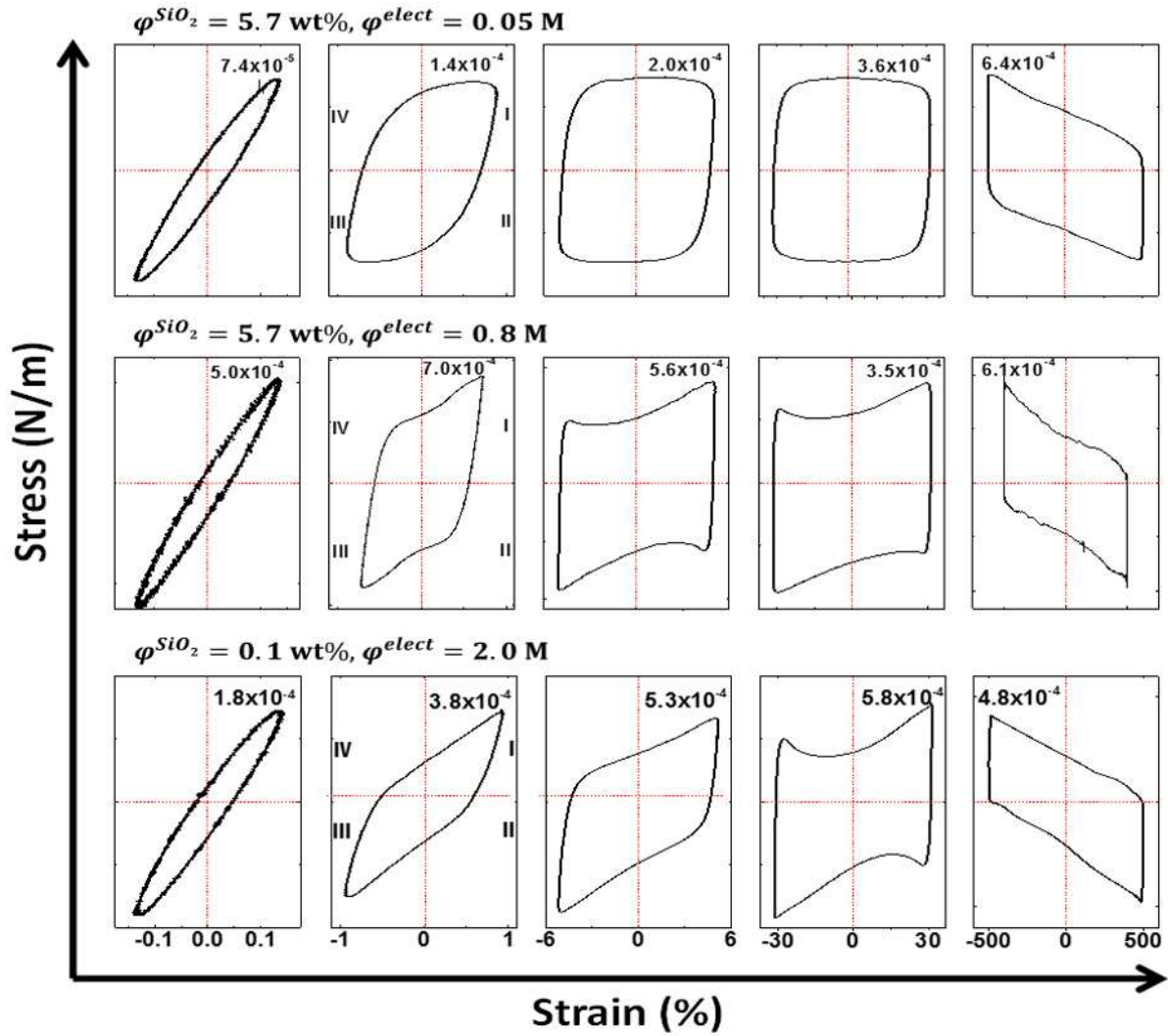
Figure 6. Lissajous plots for 5.7 wt% silica spread onto 0.05 M and 0.8 M Na_2SO_4 solutions, and 0.1 wt% silica spread onto 2.0 M Na_2SO_4 solution. Peak stress during each cycle shown in the inset of each plot.

Considering the microscopic particle motion, as schematically shown in Figure 7, at high electrolyte and particle concentrations (e.g. $\varphi^{elect} = 0.8$ M and $\varphi^{SiO_2} = 5.7$ wt%), where strong interparticle attraction exists, particles readily aggregate via the diffusion-limited cluster aggregation[23] (DLCA) process to form open, porous clusters. Under shear, beyond the first yield the attractive bridges between clusters break and the short-range adjustment of individual particles within the cluster (i.e. 'in-cage' motion) is facilitated, resulting in cluster densification, and a temporary 'shear thickening' at the strain peak within one cycle. Such effect is prominent as γ_0 increases towards the second yield point when the cages are broken. Similar phenomenon of 'strain stiffening' is also observed in cases of low φ^{SiO_2} and high φ^{elect} (e.g. $\varphi^{SiO_2} = 0.1$ wt%, $\varphi^{elect} = 2.0$ M). However, for the two-step yielding of $\varphi^{elect} =$

0.05 M and φ^{SiO_2} = 5.7 wt%, 'strain softening' dominates with the stress elongating along the x(strain)-axis at higher strain (Figure 6). The absence of strain stiffening most likely results from an inability of individual particles to undergo short-range adjustment, due to mobility restrictions resulting from the already densely packed surface aggregates formed via the reaction-limited cluster aggregation (RLCA)[23] process. Figure 7 schematically describes the microscopic responses of the two contrasting particle-laden interfaces formed either at high or intermediate φ^{elect}, where strong and relatively weak interparticle attractions dominate, respectively.
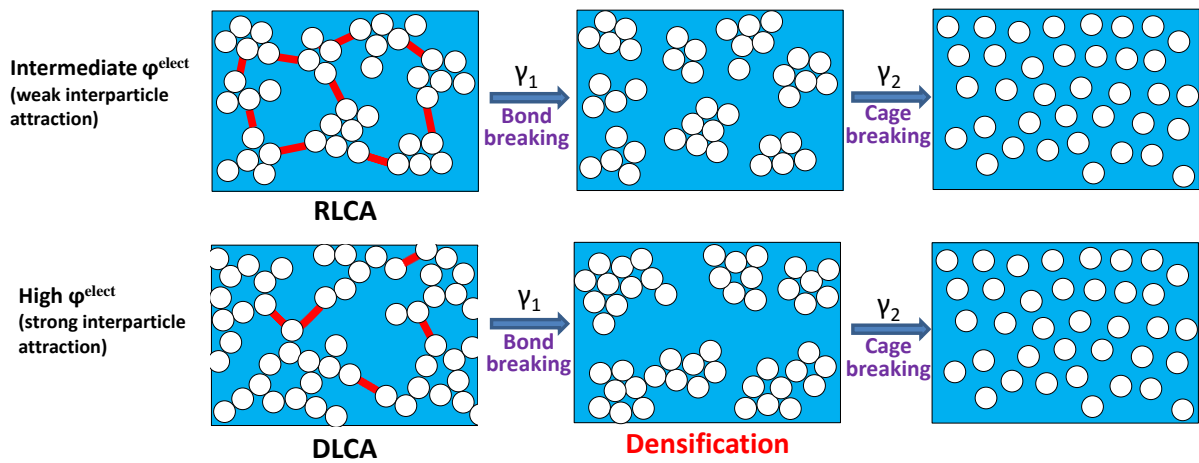

Figure 7. Top view schematic illustrating the evolution of surface particle aggregates during the two-step yielding process obtained at different φ^{elect}. Top row: two-step yielding with strain softening; bottom row: two-step-yielding with strain-stiffening. ' ▬ ' denotes the *'Bond'* between clusters

CONCLUSIONS

In summary, studying silica particle-laden interfaces as a model system with an adjustable interparticle interaction potential, the electrolyte concentration-frequency superposition is justified from the linear viscoelastic response, and the applicability of soft-glassy dynamics is confirmed. From LAOS, two-step yielding as a feature of attractive bonding and cage effects is demonstrated for the first time in colloids partitioned at the air/aqueous interface. Furthermore, microstructural rearrangement in the cage with particle displacement occurring in the shear-induced diffusivity scale has been revealed by the Lissajous curves, with either 'strain softening' or 'strain stiffening' observed between the two yielding steps, depending on

the particle interaction strength. A state diagram mapping the various phase transitions of particle-laden interfaces from fluid-like to solid-gel and to jamming glass is shown to be dependent on the two control parameters φ^{elect} and φ^{SiO_2}. With the yielding steps of the particle-laden interfaces elucidated, future efforts should be directed towards validating the micro-structural changes which occur under large strains. In practice, the research findings shed light on the flow dynamics of particles at air/liquid interfaces, which is of particular importance given the wide application of particle-stabilized interfaces in foams, emulsions and in the creation of novel materials.

Supporting Information

The Supporting Information is available free of charge on the ACS Publications website at DOI:

Details of pair-wise interaction potential between particles (Figure S1), SEM images of the Langmuir-Blodgett deposited silica particle layers at 0.05 M and 0.1 M Na_2SO_4 (Figure S2), as well as additional interfacial rheology data regarding sample pre-shear effect (Figure S3), and interfacial yielding state diagram construction (Figure S4).

REFERENCES

1.   Binks, B. P., Particles as surfactants - similarities and differences. Curr Opin Colloid In **2002,** 7, (1-2), 21-41.

2.   He, L.; Lin, F.; Li, X. G.; Sui, H.; Xu, Z. H., Interfacial sciences in unconventional petroleum production: from fundamentals to applications. Chem Soc Rev **2015,** 44, (15), 5446-5494.

3.   Aranberri, I.; Binks, B. P.; Clint, J. H.; Fletcher, P. D. I., Synthesis of macroporous silica from solid-stabilised emulsion templates. J Porous Mat **2009,** 16, (4), 429-437.

4.   Lin, Y.; Skaff, H.; Emrick, T.; Dinsmore, A. D.; Russell, T. P., Nanoparticle assembly and transport at liquid-liquid interfaces. Science **2003,** 299, (5604), 226-229.

5.   Yuan, Q. C.; Cayre, O. J.; Fujii, S.; Armes, S. P.; Williams, R. A.; Biggs, S., Responsive Core-Shell Latex Particles as Colloidosome Microcapsule Membranes. Langmuir **2010,** 26, (23), 18408-18414.

6.   Sanz, E.; White, K. A.; Clegg, P. S.; Cates, M. E., Colloidal Gels Assembled via a Temporary Interfacial Scaffold. Phys Rev Lett **2009,** 103, (25).

7.   Ikem, V. O.; Menner, A.; Bismarck, A., High Internal Phase Emulsions Stabilized Solely by Functionalized Silica Particles. Angew Chem Int Edit **2008,** 47, (43), 8277-8279.

8.   Neirinck, B.; Fransaer, J.; Van der Biest, O.; Vleugels, J., Production of porous materials through consolidation of Pickering emulsions. Adv Eng Mater **2007,** 9, (1-2), 57-59.

9.	Erni, P.; Parker, A., Nonlinear Viscoelasticity and Shear Localization at Complex Fluid Interfaces. Langmuir **2012,** 28, (20), 7757-7767.

10.	Stone, H. A.; Koehler, S. A.; Hilgenfeldt, S.; Durand, M., Perspectives on foam drainage and the influence of interfacial rheology. J Phys-Condens Mat **2003,** 15, (1), S283-S290.

11.	Lexis, M.; Willenbacher, N., Yield stress and elasticity of aqueous foams from protein and surfactant solutions - The role of continuous phase viscosity and interfacial properties. Colloid Surface A **2014,** 459, 177-185.

12.	Lexis, M.; Willenbacher, N., Relating foam and interfacial rheological properties of beta-lactoglobulin solutions. Soft Matter **2014,** 10, (48), 9626-9636.

13.	Safinia, L.; Wilson, K.; Mantalaris, A.; Bismarck, A., Through-thickness plasma modification of biodegradable and nonbiodegradable porous polymer constructs. J Biomed Mater Res A **2008,** 87A, (3), 632-642.

14.	Bismarck, A., Are hierarchical composite structures the way forward to improve the properties of truly green composites? Express Polym Lett **2008,** 2, (10), 687-687.

15.	Pham, K. N.; Petekidis, G.; Vlassopoulos, D.; Egelhaaf, S. U.; Poon, W. C. K.; Pusey, P. N., Yielding behavior of repulsion- and attraction-dominated colloidal glasses. J Rheol **2008,** 52, (2), 649-676.

16.	Zhou, Z.; Hollingsworth, J. V.; Hong, S.; Cheng, H.; Han, C. C., Yielding Behavior in Colloidal Glasses: Comparison between "Hard Cage" and "Soft Cage". Langmuir **2014,** 30, (20), 5739-5746.

17.	Derjaguin, B.; Landau, L., Theory of the stability of strongly charged lyophobic sols and of the adhesion of strongly charged particles in solutions of electrolytes. Acta Physico Chemica URSS **1941,** 14.

18.	Verwey, E. J. W.; Overbeek, J. T. G., Theory of the stability of lyophobic colloids. Elsevier Amsterdam, 1948.

19.	Pusey, P. N.; Vanmegen, W., Observation of a Glass-Transition in Suspensions of Spherical Colloidal Particles. Phys Rev Lett **1987,** 59, (18), 2083-2086.

20.	Koumakis, N.; Petekidis, G., Two step yielding in attractive colloids: transition from gels to attractive glasses. Soft Matter **2011,** 7, (6), 2456-2470.

21.	Webber, G. B.; Wanless, E. J.; Butun, V.; Armes, S. P.; Biggs, S., Self-organized monolayer films of stimulus-responsive micelles. Nano Lett **2002,** 2, (11), 1307-1313.

22.	Reynaert, S.; Moldenaers, P.; Vermant, J., Interfacial rheology of stable and weakly aggregated two-dimensional suspensions. Phys Chem Chem Phys **2007,** 9, (48), 6463-6475.

23.	Mewis, J. W., Norman J., Colloidal Suspension Rheology. Cambridge University Press: New York, 2012.

24.	Cicuta, P.; Stancik, E. J.; Fuller, G. G., Shearing or compressing a soft glass in 2D: Time-concentration superposition. Phys Rev Lett **2003,** 90, (23).

25.	Zang, D. Y.; Rio, E.; Langevin, D.; Wei, B.; Binks, B. P., Viscoelastic properties of silica nanoparticle monolayers at the air-water interface. Eur Phys J E **2010,** 31, (2), 125-134.

26.	Tran, M. Q.; Cabral, J. T.; Shaffer, M. S. P.; Bismarck, A., Direct measurement of the wetting behavior of individual carbon nanotubes by polymer melts: The key to carbon nanotube-polymer composites. Nano Lett **2008,** 8, (9), 2744-2750.

27.   Harbottle, D.; Chen, Q.; Moorthy, K.; Wang, L. X.; Xu, S. M.; Liu, Q. X.; Sjoblom, J.; Xu, Z. H., Problematic Stabilizing Films in Petroleum Emulsions: Shear Rheological Response of Viscoelastic Asphaltene Films and the Effect on Drop Coalescence. Langmuir **2014,** 30, (23), 6730-6738.

28.   Pradilla, D.; Simon, S.; Sjoblom, J.; Samaniuk, J.; Skrzypiec, M.; Vermant, J., Sorption and Interfacial Rheology Study of Model Asphaltene Compounds. Langmuir **2016,** 32, (12), 2900-2911.

29.   Kostakis, T.; Ettelaie, R.; Murray, B. S., Effect of high salt concentrations on the stabilization of bubbles by silica particles. Langmuir **2006,** 22, (3), 1273-1280.

30.   Maestro, A.; Deshmukh, O. S.; Mugele, F.; Langevin, D., Interfacial Assembly of Surfactant-Decorated Nanoparticles: On the Rheological Description of a Colloidal 2D Glass. Langmuir **2015,** 31, (23), 6289-6297.

31.   Aveyard, R.; Binks, B. P.; Clint, J. H.; Fletcher, P. D. I.; Horozov, T. S.; Neumann, B.; Paunov, V. N.; Annesley, J.; Botchway, S. W.; Nees, D.; Parker, A. W.; Ward, A. D.; Burgess, A. N., Measurement of long-range repulsive forces between charged particles at an oil-water interface. Phys Rev Lett **2002,** 88, (24).

32.   Ewoldt, R. H.; Hosoi, A. E.; McKinley, G. H., New measures for characterizing nonlinear viscoelasticity in large amplitude oscillatory shear. J Rheol **2008,** 52, (6), 1427-1458.

33.   Hyun, K.; Wilhelm, M.; Klein, C. O.; Cho, K. S.; Nam, J. G.; Ahn, K. H.; Lee, S. J.; Ewoldt, R. H.; McKinley, G. H., A review of nonlinear oscillatory shear tests: Analysis and application of large amplitude oscillatory shear (LAOS). Prog Polym Sci **2011,** 36, (12), 1697-1753.

34.   Koumakis, N.; Brady, J. F.; Petekidis, G., Complex Oscillatory Yielding of Model Hard-Sphere Glasses. Phys Rev Lett **2013,** 110, (17).

35.   Jacob, A. R.; Poulos, A. S.; Kim, S.; Vermant, J.; Petekidis, G., Convective Cage Release in Model Colloidal Glasses. Phys Rev Lett **2015,** 115, (21).

36.   Keim, N. C.; Arratia, P. E., Mechanical and Microscopic Properties of the Reversible Plastic Regime in a 2D Jammed Material. Phys Rev Lett **2014,** 112, (2).

37.   Srinivasan, S.; McKinley, G. H.; Cohen, R. E., Assessing the Accuracy of Contact Angle Measurements for Sessile Drops on Liquid-Repellent Surfaces. Langmuir **2011,** 27, (22), 13582-13589.

38.   Vandebril, S.; Franck, A.; Fuller, G. G.; Moldenaers, P.; Vermant, J., A double wall-ring geometry for interfacial shear rheometry. Rheol Acta **2010,** 49, (2), 131-144.

39.   Williams, D. F.; Berg, J. C., The Aggregation of Colloidal Particles at the Air-Water-Interface. J Colloid Interf Sci **1992,** 152, (1), 218-229.

40.   Chen, W.; Tan, S. S.; Zhou, Y.; Ng, T. K.; Ford, W. T.; Tong, P., Attraction between weakly charged silica spheres at a water-air interface induced by surface-charge heterogeneity. Phys Rev E **2009,** 79, (4).

41.   Masschaele, K.; Park, B. J.; Furst, E. M.; Fransaer, J.; Vermant, J., Finite Ion-Size Effects Dominate the Interaction between Charged Colloidal Particles at an Oil-Water Interface. Phys Rev Lett **2010,** 105, (4).

42.   Park, B. J.; Pantina, J. P.; Furst, E. M.; Oettel, M.; Reynaert, S.; Vermant, J., Direct measurements of the effects of salt and surfactant on interaction forces between colloidal particles at water-oil interfaces. Langmuir **2008,** 24, (5), 1686-1694.

43.   Hurd, A. J., The Electrostatic Interaction between Interfacial Colloidal Particles. J Phys a-Math Gen **1985,** 18, (16), 1055-1060.

44.   Frydel, D.; Dietrich, S.; Oettel, M., Charge renormalization for effective interactions of colloids at water interfaces. Phys Rev Lett **2007,** 99, (11).

45.   Wirth, C. L.; Furst, E. M.; Vermant, J., Weak Electrolyte Dependence in the Repulsion of Colloids at an Oil-Water Interface. Langmuir **2014,** 30, (10), 2670-2675.

46.   Petkov, P. V.; Danov, K. D.; Kralchevsky, P. A., Mono layers of charged particles in a Langmuir trough: Could particle aggregation increase the surface pressure? J Colloid Interf Sci **2016,** 462, 223-234.

47.   Garbin, V.; Crocker, J. C.; Stebe, K. J., Nanoparticles at fluid interfaces: Exploiting capping ligands to control adsorption, stability and dynamics. J Colloid Interf Sci **2012,** 387, 1-11.

48.   Trappe, V.; Weitz, D. A., Scaling of the viscoelasticity of weakly attractive particles. Phys Rev Lett **2000,** 85, (2), 449-452.

49.   Srivastava, S.; Leiske, D.; Basu, J. K.; Fuller, G. G., Interfacial shear rheology of highly confined glassy polymers. Soft Matter **2011,** 7, (5), 1994-2000.

50.   Van Hooghten, R.; Imperiali, L.; Boeckx, V.; Sharma, R.; Vermant, J., Rough nanoparticles at the oil-water interfaces: their structure, rheology and applications. Soft Matter **2013,** 9, (45), 10791-10798.

51.   Sollich, P.; Lequeux, F.; Hebraud, P.; Cates, M. E., Rheology of soft glassy materials. Phys Rev Lett **1997,** 78, (10), 2020-2023.

52.   Sollich, P., Rheological constitutive equation for a model of soft glassy materials. Phys Rev E **1998,** 58, (1), 738-759.

53.   Wen, Y. H.; Schaefer, J. L.; Archer, L. A., Dynamics and Rheology of Soft Colloidal Glasses. ACS Macro Lett **2015,** 4, (1), 119-123.

54.   Zong, Y. W.; Yuan, G. C.; Zhao, C. Z.; Han, C. C., Differentiating bonding and caging in a charged colloid system through rheological measurements. J Chem Phys **2013,** 138, (18).

55.   Moncho-Jorda, A.; Martinez-Lopez, F.; Gonzalez, A. E.; Hidalgo-Alvarez, R., Role of long-range repulsive interactions in two-dimensional colloidal aggregation: Experiments and simulations. Langmuir **2002,** 18, (24), 9183-9191.

Table of Contents Graphic